International Journal of Nanomedicine

Dovepress
Taylor & Francis Group

Open Access Full Text Article

ORIGINAL RESEARCH

Honeysuckle-Derived Exosome-Like Nanovesicles Protect Against Acute Liver Failure by Modulating Gut Microbiota

Ping Li[1–3], Yan Tang[1,3,4], Yixun Chen[1,3,4], Weijiao Fan[1,3], Jiayu Yao[1,3], Kexin Yu[1,3], Yiyi Shan[1,3], Jie Wang[5], Xiang Ming Ye[1], Hai Zou[6], Xiaozhou Mou[1,3]

[1]Center for Rehabilitation Medicine, Rehabilitation and Sports Medicine Research Institute of Zhejiang Province, Department of Rehabilitation Medicine, Zhejiang Provincial People's Hospital (Affiliated People's Hospital), Hangzhou Medical College, Hangzhou, People's Republic of China; [2]College of Pharmaceutical Sciences, Zhejiang University of Technology, Hangzhou, People's Republic of China; [3]Clinical Research Institute, Zhejiang Provincial People's Hospital (Affiliated People's Hospital), Hangzhou Medical College, Hangzhou, People's Republic of China; [4]College of Life Sciences, Zhejiang Chinese Medical University, Hangzhou, People's Republic of China; [5]EVital Bio (Hangzhou) Co., Ltd, Hangzhou, People's Republic of China; [6]Department of Critical Care, Shanghai Cancer Center, Fudan University, Shanghai, People's Republic of China

Correspondence: Hai Zou; Xiaozhou Mou, Email zouhai@fudan.edu.cn; mouxz@zju.edu.cn

Purpose: Acute liver failure (ALF) is a rare but life-threatening condition caused by drug toxicity, viral infections, or autoimmune disorders. Current treatments rely heavily on liver transplantation, which is costly and high-risk. As most therapies target single mechanisms, developing safe, cost-effective multi-target drugs is urgently needed.

Methods: In this study, we isolated exosome-like nanovesicles from dried honeysuckle (HNVs) and evaluated their therapeutic potential in a lipopolysaccharide/D-galactosamine (LPS/GalN)-induced ALF mouse model. We first characterized HNVs using cryo-electron microscopy (Cryo-EM), transmission electron microscopy (TEM), and dynamic light scattering (DLS), and confirmed their stability in gastrointestinal simulation fluid in vivo. Subsequently, we validated the biological safety and in vivo distribution of HNVs in mice. Afterwards, we constructed an ALF model and tested the therapeutic efficacy of HNVs on this model. Through RNA sequencing, 16S rRNA analysis, and complementary techniques such as Western blot and quantitative real-time PCR, we elucidated the underlying mechanisms of HNVs in mitigating ALF.

Results: Our results showed that HNVs significantly ameliorated the pathological symptoms associated with ALF mice. Specifically, HNVs induced a significant 1.89-fold decrease in serum ALT levels and a 1.95-fold decrease in AST levels. HNVs also ameliorated the hepatocellular necrosis and inflammatory cell infiltration caused by LPS/GalN. In addition, our findings suggest that the mechanism by which HNVs ameliorate ALF is: (1) they directly target the liver by traversing the compromised intestinal barrier, suppressing hepatic immune-inflammatory responses, and ameliorating ALF; (2) they restore intestinal barrier integrity by modulating the gut microbiota, thus reducing the translocation of gut-derived LPS to the liver and preventing further hepatic injury.

Conclusion: In summary, we developed a novel natural nanomedicine with dual-targeting capabilities and demonstrated its efficacy against ALF, offering a promising therapeutic alternative for this severe condition.

Keywords: acute liver failure, Honeysuckle-derived exosome-like nanovesicles, gut microbiota, immune-inflammatory responses

Introduction

Acute liver failure (ALF) is a rare but highly lethal clinical syndrome whose causes include viral infections, drug or toxin damage, or autoimmune diseases. Liver transplantation is the only effective treatment, but only a limited proportion of patients can receive a liver transplant due to a shortage of donors.[1–3] Thus, there is an urgent need to produce medications that are safe, effective, and conveniently available. To investigate the pathophysiology of ALF, it is crucial to establish a suitable animal model. Lipopolysaccharide (LPS) combined with D-galactosamine (D-GalN)-induced ALF model is a classical approach to explore the pathogenesis of ALF.[4] Rodents are not susceptible to LPS administration alone, and the majority of deaths are caused by LPS-induced hypotensive shock rather than hepatic injury; however, D-GalN can only

Received: 7 March 2025
Accepted: 2 October 2025
Published: 25 October 2025

be processed by the liver, and concurrent administration of D-GalN increases the animal's susceptibility to LPS. LPS triggers Kupffer polarization towards M1 macrophages and promotes the release of inflammatory factors by activating TLR4 receptors on hepatic Kupffer cells, leading to massive hepatocyte injury and necrosis.[5] However, the complexity of ALF lies in the fact that it is often accompanied by a systemic cytokine storm, which disrupts the intestinal barrier and triggers disruption of the intestinal microbiota.[6,7] This disruption in turn leads to the entry of gut-derived LPS into the liver, exacerbating the hepatic immune-inflammatory response and creating a vicious cycle of the "gut-liver axis".[8,9] Conventional intervention strategies tend to focus on a single pathomechanism (eg, suppression of inflammation or modulation of the intestinal microbiota),[10,11] but it is difficult to address the intertwined immune dysregulation and microecological imbalance in ALF. Therefore, the construction of a synergistic therapeutic system that synchronously regulates the pathological nodes of multiple systems has become the key to break through the bottleneck.

Honeysuckle, a traditional herb, is known for its hepatoprotective and choleretic properties.[12] The latest research shows that honeysuckle has excellent anti-inflammatory and gut microbiota regulating properties.[13,14] Plant-derived exosome-like nanovesicles (PELNVs) are bioactive materials derived from plants, containing various active ingredients such as proteins, lipids, small RNAs, and others.[15] Studies have shown that PELNVs exhibit efficacy comparable to or superior to that of the original plants. Furthermore, PELNVs not only overcome the poor biosafety and complex preparation processes associated with traditional nanomedicines but also demonstrate higher production yields and better biocompatibility than animal-derived exosome-like nanovesicles.[16–18] What is more, PELNVs have demonstrated therapeutic efficacy in various animal models. For instance, lemon-derived exosomes accelerate diabetic wound healing,[19] while Houttuynia cordata exosomes effectively alleviate colitis.[20] Ginseng exosomes have also shown potential in glioma treatment.[21] Additionally, PELNVs exhibit superior suitability for oral administration due to their resistance to harsh gastrointestinal conditions.[22] Recent studies further reveal that orally administered PELNVs can persist in the gut for prolonged periods, thereby enabling therapeutic effects on liver diseases through modulation of the gut microbiota.[23]

Therefore, we extracted exosome-like nanovesicles from dried flowers of Honeysuckle (HNVs) and validated the efficacy on an ALF model established by LPS/GalN. Our study demonstrated for the first time that HNVs were able to inhibit both gut-derived and exogenous LPS, suppressing the hepatic immune-inflammatory response and ultimately improving ALF (Scheme 1).

Experiment Section

Preparation and Characterization of HNVs

Dried honeysuckle were bought from Tong Ren Tang, a traditional Chinese medicine merchant. Dried honeysuckle was soaked in phosphate buffer solution (PBS) for 30 min, followed by thorough homogenization using a tissue homogenizer. The homogenate was centrifuged at 10,000 rpm for 60 min and the precipitate was discarded. This centrifugation process was repeated several times until the supernatant was free of precipitate visible to the naked eye. The supernatants from multiple centrifugations were combined and used as samples to be processed prior to purification. The above samples were injected into the an Unique AutoTFF075-M Crossflow filtration system (Inscinstech, Suzhou, China) and flowed sequentially through a hollow fiber column with a pore size of 200 nm and a molecular weight cut-off of 750 kDa (CleaSep® Hollow Fiber Filter, HFELA750100640, Membrane Solutions (Nantong) Co. Ltd, China) for hierarchical separation. Fractions with particle size ≤200 nm and particle size >750 kDa, defined as HNVs, were finally collected. The BCA Protein Concentration Kit (P0012, Beyotime) was used to measure the protein concentration of HNVs. The HNVs were resuspended in double-distilled water and characterized for their particle size and zeta potential using dynamic light scattering (DLS). Transmission electron microscopy (TEM) and cryo-electron microscopy (Cryo-EM) were used to investigate their shape.

Stability of Gastrointestinal Fluids of HNVs

HNVs were suspended in artificial simulated gastric fluid (PH1840, Phygene) and artificial simulated intestinal fluid (PH1841, Phygene) respectively, adjusted to a final concentration of 0.1 mg/mL. After two-hour incubation at 37°C, the solutions were characterized by TEM for morphological analysis and by DLS for particle size measurement.

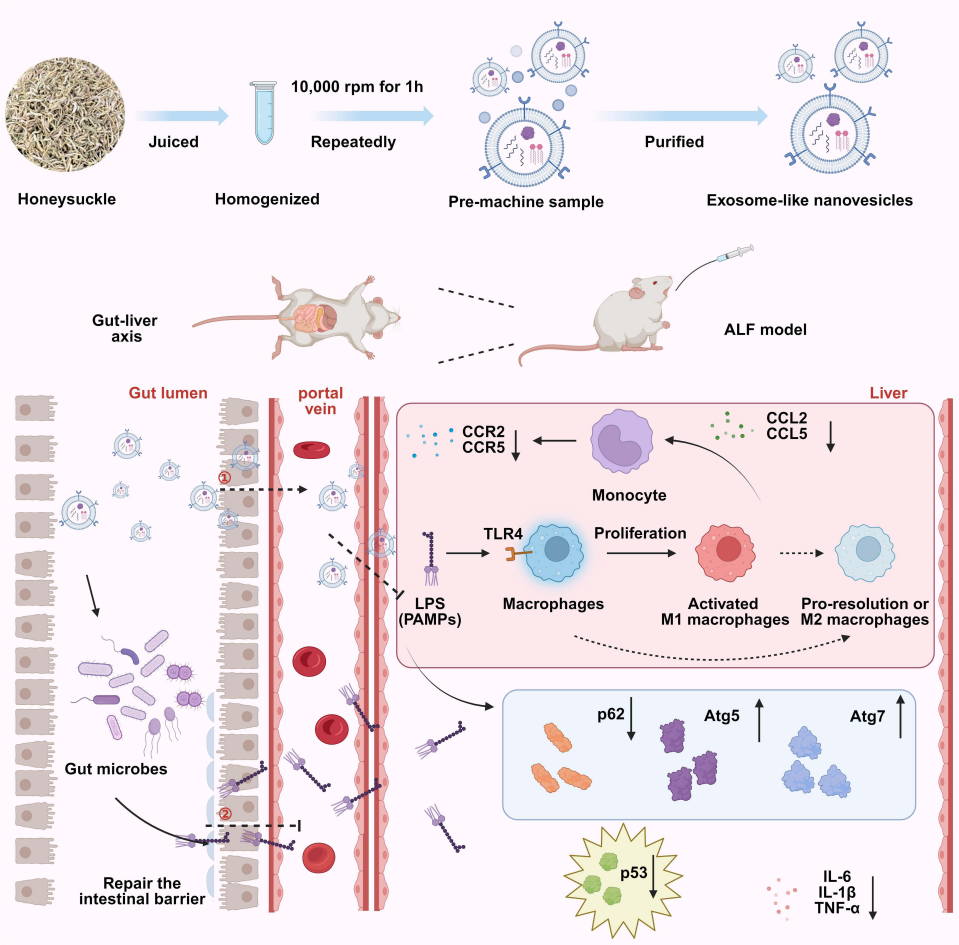

Scheme 1 Preparation process of HNVs and its mechanism to improve ALF.

Cell Culture

HepG2 (human hepatocellular carcinoma cells) were obtained from Meisen Chinese Tissue Culture Collections (Jinhua, China). The cells were cultured in Dulbecco's Modified Eagle Medium (DMEM) supplemented with 10% FBS (Hangzhou Yangming Biotechnology Co., Ltd)., 100 U/mL penicillin, and 100 μg/mL streptomycin. All cultures were maintained at 37°C in a 5% CO_2 atmosphere.

Cell Viability Test

Cell suspensions were seeded into 96-well plates at 100 μL per well. The cells were then divided into seven treatment groups: HNVs dose groups (50, 100, 150, 200, 250, and 300 μg/mL) and a blank control group. Each group contained five replicate wells. Following 24-hour incubation at 37°C, 10% CCK-8 reagent in DMEM was added to each well. After 2-hour incubation in a thermostat and shielded from light, absorbance was measured at 450 nm.

In vivo Distribution Experiments of HNVs

Following the instructions, the DIR (Yeasen, Shanghai, China) and HNVs were incubated in a thermostatic incubator at 37°C for 30 minutes. They were then moved into ultrafiltration centrifuge tubes and centrifuged at 3000 g for twenty minutes. The solution's top layer was then identified as the DIR-labeled HNVs. Twelve mice were randomly divided into two groups of six. The model group received intraperitoneal injections of LPS (100 μg/kg) and GalN (700 mg/kg), while the control group received an intraperitoneal injection of PBS. After an hour, oral gavage of 50 mg/kg of HNVs was given to each mouse individually. At the designated intervals, the mice were then dissected, and the heart, liver, spleen,

https://doi.org/10.2147/IJN.S526819

lung, kidney, and intestine were obtained. Following saline washing, the distribution of DIR-labeled HNVs in control and model mice was shown in a animal imaging system.

HNVs Biosafety Experiments

Twelve BALB/c mice (6–8 weeks) were split into four groups at random. Three of the groups received oral gavage treatments of 25 mg/kg, 50 mg/kg, and 100 mg/kg of HNVs, while the fourth group received oral gavage treatment of 200 μL of PBS, once a day for 5 days, body weights of all animals were recorded daily, and at the end of the experiment, all mice were euthanized, and hearts, livers, spleens, lungs, kidneys, and serum were collected.

Animal Experiment

All animal experiments were conducted in accordance with the Guidelines for Ethical Review of Laboratory Animal Welfare published by China (GB/T 35892–2018) and were approved by the Zhejiang Provincial People's Hospital Ethics Committee. Male BALB/c mice (6–8 weeks old) were sourced from GemPharmatech Co. Unless otherwise noted, mice were allowed unrestricted access to food and water, and the room temperature was kept at 22°C with 50% humidity and a 12-hour light/dark cycle. LPS (L6529, sigma-aldrich) and D-GalN (ST1213, Beyotime) were injected intraperitoneally into mice to create a model of ALF. Based on the results of the biosafety evaluation, ie, HNVs maintain good biosafety in the range of 25 mg/kg-100 mg/kg, hence, mice in the treatment group received oral gavage of HNVs (50 mg/kg) one hour after the ALF model was established, whereas mice in the control group were gavaged with identical doses of PBS. Mice were euthanized six hours following successful ALF modeling, and serum, liver, and the contents of cecum were collected.

Serum Biochemical Assay

Serum levels of ALT, AST, BUN, and Cr were measured using a fully automated biochemical analyzer. Concentrations of IL-6 (JL20268, JONLNBIO), IL-1β (JL18442, JONLNBIO), and TNF-α (JL10484, JONLNBIO) in mouse serum were determined by enzyme-linked immunosorbent assay (ELISA) according to the manufacturers' instructions. Absorbance was measured at 450 nm, and sample concentrations were calculated using standard curves.

Histopathological Analysis

HE staining is used to evaluate the histopathologic condition of mice. 4% paraformaldehyde was used to fix the tissues of the mice. Following dehydration and transparency, the tissue was paraffin-embedded and prepared into paraffin sections. Eosin and Hematoxylin were then used to stain the tissues' cytoplasm and nuclei, respectively, following the dewaxing of the paraffin. Immunofluorescence staining was performed to analyze macrophage polarization and apoptosis (via TUNEL assay) in mouse liver tissues. Following deparaffinization and rehydration of paraffin sections, nonspecific binding was blocked with goat serum. Sections were then incubated sequentially with primary and secondary antibodies. Fluorescence images were acquired using laser scanning confocal microscopy and analyzed quantitatively with ImageJ software.

Liver RNA-Seq

Following tissue RNA extraction, an Agilent 2100 bioanalyzer was used to assess the integrity of the RNA. The mRNA containing polyA tails was then enriched using Oligo(dT) magnetic beads. The purified mRNA was then fragmented using divalent cations, and first-strand cDNA was synthesized with the fragmented mRNA as template. A cDNA library was constructed by processing the purified double-stranded cDNA through size selection, PCR amplification, and purification. Library insert size was validated using the Agilent 2100 Bioanalyzer. Upon successful quality assessment, sequencing was performed on an Illumina platform.

Extraction of Liver Primary Cells and Flow Cytometry

Mice were anesthetized and blood was flushed from the liver using Hank's Balanced Salt Solution (abs9258, Absin). After significant swelling of the liver was observed, the portal vein was clipped and the superior vena cava was clamped until the liver became completely white. The liver was then flushed with collagenase (abs47048000, Absin) until it became loose. The liver was clipped to 10 mL of collagenase A solution (to which 1% DNase I had been added) and gently shaken for 10

min in a 37°C water bath, then pre-cooled HBSS solution was quickly added to 50 mL, and 200 μL of DNase I solution was added and then mixed well. After passing through a 70 μm cell filter, the mixture was centrifuged at 500 g for 7 minutes. The precipitate was recovered, including the total liver cells. Total liver cells were resuspended and centrifuged at 100 g for 5 minutes, and the supernatant was collected; these were the liver nonparenchymal cells. The resultant supernatant was centrifuged at 500 g for 7 minutes, and the precipitate, which consisted of liver nonparenchymal cells, was collected. In a 1:5 ratio, Red Blood Cell Lysis Buffer lysate (abs9101, Absin) was added to the precipitate obtained above. The mixture was then centrifuged at 500 g for 7 minutes at 4°C. The precipitate was then gathered and resuspended in HBSS. Fixable Viability Stain 510 (564406, Becton, Dickinson and Company) was added to the resuspension to exclude non-viable cells and FcBlock (553141, Becton, Dickinson and Company) was added to remove non-specific binding. Next, CD45 (557659, Becton, Dickinson and Company), CD11b (557396, Becton, Dickinson and Company), F4/80 (565410, Becton, Dickinson and Company), CD11c (558079, Becton, Dickinson and Company), and CD206 (565250, Becton, Dickinson and Company) were added according to the reagent manufacturer's instructions. An Agilent-NovoCyte Penteon instrument was used to collect the data, and NovoExpress software was then used for analysis.

Western Blot

Weigh 20 mg of tissue sample, add two stainless steel beads and 200 μL RIPA lysis buffer. Following homogenization at 60 Hz for 60s (three cycles) using a tissue grinder, samples were centrifuged at 12,000 rpm for 20 minutes to collect supernatant. Proteins were separated and transferred to PVDF membranes. After blocking membranes with 5% skim milk for two hours, primary antibody incubation was performed overnight at 4°C with shaking. Membranes were then incubated with secondary antibody, and protein signals were detected using Image Lab software.

The following primary antibodies were employed: Marker (RM19001, ABclonal), Beta Actin Polyclonal antibody (20536-1-AP, Proteintech), GAPDH (10494-1-AP, Proteintech), Atg7 (A19604, ABclonal), Atg5 (A19677, ABclonal), P53 (2524T, Cell Signaling Technology), P62 (16177T, Cell Signaling Technology).

Quantitative Real-Time PCR

Following the manufacturer's guidelines, total RNA was extracted from tissues using TRIzol reagent, and NanoDrop was used to assess the RNA's quality and purity. The isolated RNA was reverse transcribed to cDNA with the cDNA Synthesis SuperMix kit (NovoProtein Technology, China). Quantitative real-time PCR was subsequently performed using primer sequences listed in Table S1.

16S rRNA Sequencing

The FastPure Stool DNA Isolation Kit (Majorbio, Shanghai, China) was used to extract the whole genomic DNA of the microbial communities present in the cecum contents. 1% agarose gel electrophoresis was used to detect the integrity of DNA. The concentration and purity of the isolated DNA were assessed using Nanodrop2000. The V3-V4 variable region of the 16s rRNA gene was amplified by PCR using the isolated DNA mentioned above as a template. 338F (5′-ACTCCTACGGGGAGGCAGCAG-3′) was the upstream primer, while 806R (5′-GGACTACHVGGGGTWTCTAAT-3′) was the downstream primer. The sequencing procedure was carried out using Illumina Miseq PE300 platform. The high-throughput 16S rRNA sequencing was performed in Majorbio Bio-Pharm Technology Co. Ltd. The data were analyzed on the free online platform of I-Sanger Cloud Platform.

Statistical Analyses

Statistical analyses were performed using GraphPad Prism software, version 9.0. Comparisons among multiple groups were conducted through one-way ANOVA, followed by Dunnett's T3 test for multiple comparisons. The means of the two groups were compared using *t*-test. In all figures, error bars indicate the standard deviation (SD). * $P < 0.05$, ** $P < 0.01$, n.s., not significant vs Model group.

Results

Preparation and Characterization of HNVs

Dried honeysuckle was subjected to juice extraction, centrifugation, and purification to obtain HNVs (Figure 1A). To investigate the morphology of HNVs, we used cryo-EM. Based on cryo-EM imaging (Figure 1B), HNVs appeared as

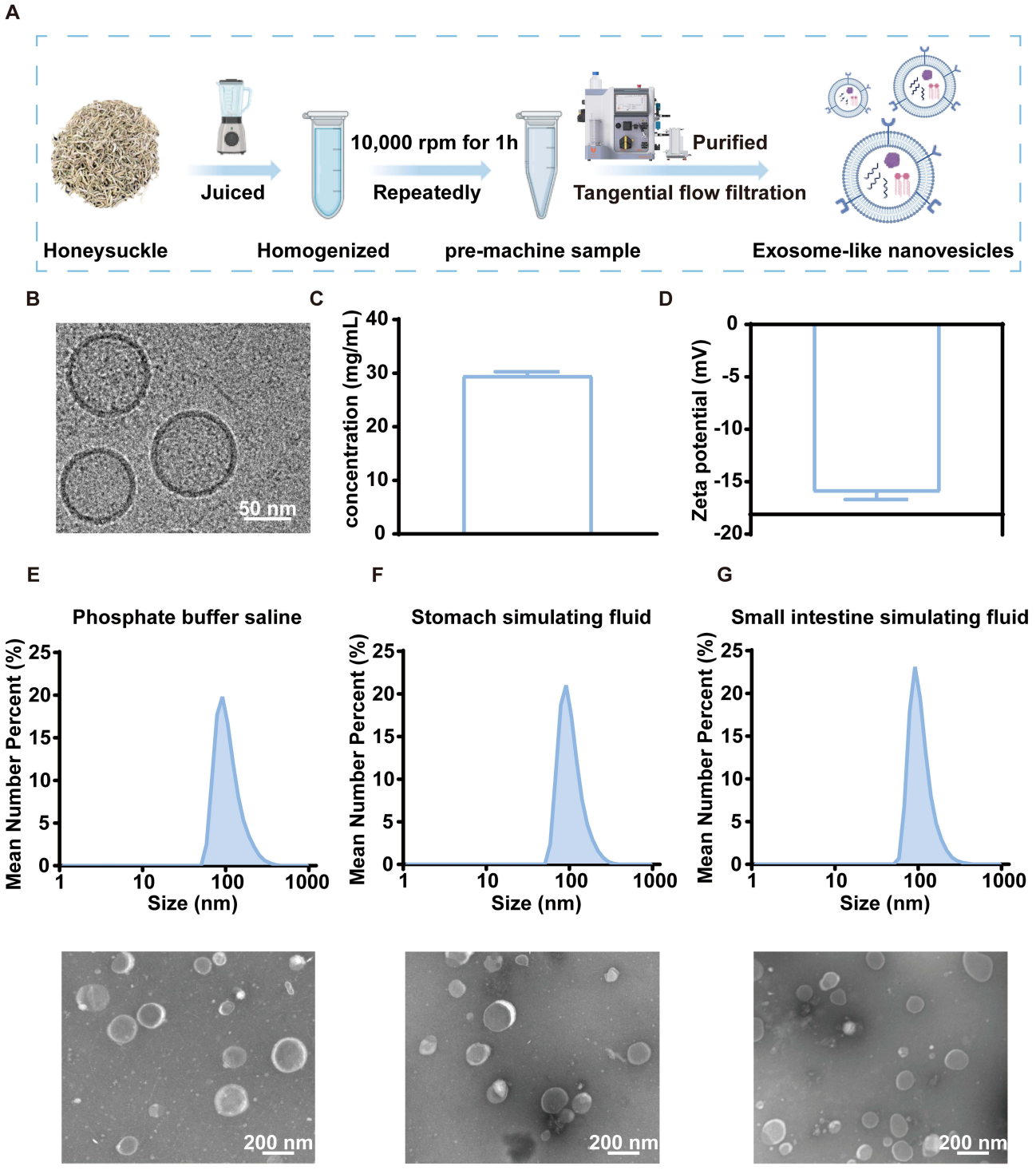

Figure 1 Preparation and characterization of HNVs. (**A**) Flowchart of HNVs preparation. (**B**) Cryo-EM images of HNVs. (**C**) Protein concentration of HNVs (n=3). (**D**) Zeta potential of HNVs (n=3). (**E**) Particle size distribution and TEM images of HNVs in PBS. (**F**) Particle size distribution and TEM images of HNVs in Stomach simulating fluid. (**G**) Particle size distribution and TEM images of HNVs in Small intestine simulating fluid. Data were expressed as the mean ± SD.

individual exosome-like nanovesicles with spherical morphology and a particle size distribution ranging from 50 to 200 nm. To quantify HNVs, we employed the BCA assay to measure protein content. We found that 1 mL of HNVs could be obtained from 8 g of dried honeysuckle, with a protein concentration of 29.47 mg/mL (Figure 1C). The zeta potential of HNVs was measured using DLS, revealing a negative value of −15.97 mV (Figure 1D). To simulate gastrointestinal stability in vivo, HNVs were incubated for 2 hours in each of the following media: PBS (Figure 1E), Stomach simulating fluid (Figure 1F), and Small intestine simulating fluid (Figure 1G). The morphology and particle size distribution of HNVs were subsequently characterized by TEM and DLS. We found that the particle sizes of HNVs in PBS, Stomach simulating fluid and Small intestine simulating fluid were distributed around 158.5 nm, 147.4 nm,164.5 nm, respectively, and the HNVs were able to maintain a spherical morphology after 2 hours of incubation, which indicated that the HNVs had good stability.

In vivo Distribution Experiment of HNVs

Prior to evaluating HNVs' therapeutic potential against ALF, we compared the in vivo biodistribution of DIR-labeled HNVs in ALF versus control mice (Figure 2A and B). DIR-labeled HNVs were used to track the distribution of HNVs in vivo, and we found that HNVs could be taken up by ALF mice. HNVs entered the intestine after two hours and then progressively made their way into the liver, reaching their maximum accumulation in the liver of ALF animals at four hours. As a comparison, in the Control group, HNVs similarly entered the intestine at 2 hours. Nevertheless, in the control group, we discovered that HNVs were unable to enter the liver, and we hypothesize that this could be connected to the intestinal barrier disruption in ALF mice.

Biosafety Evaluation of HNVs

The foundation of clinical translation requires demonstrated biosafety. BALB/c mice (6–8 weeks old) were divided into four groups: PBS control, HNVs low-dose (25 mg/kg), HNVs medium-dose (50 mg/kg), and HNVs high-dose (100 mg/kg).

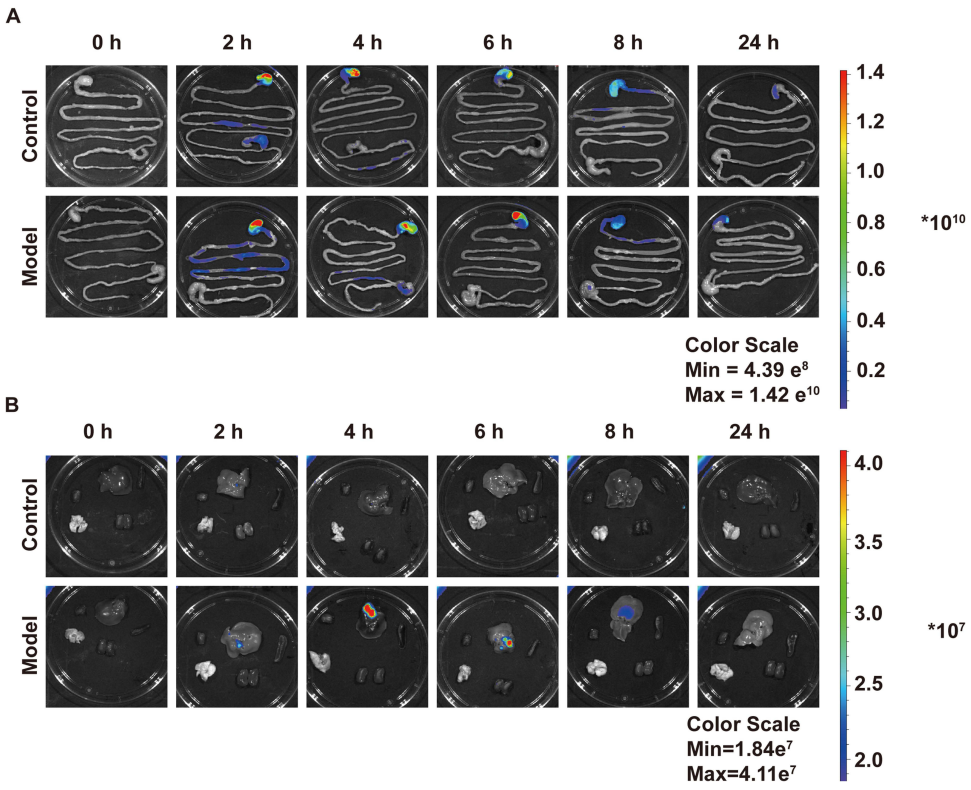

Figure 2 Fluorescence distribution images of control and model groups at various time points following oral treatment of HNVs. (**A**) Images of fluorescence distribution of HNVs at various times in the intestines of mice in the Control and Model groups. (**B**) Images of fluorescence distribution of HNVs at various times in major organs of mice in the Control and Model groups.

https://doi.org/10.2147/IJN.S526819

Mice received daily oral administrations of their respective treatments for five consecutive days, with body weights monitored throughout. No significant changes in body weight were observed in any HNVs-treated group compared to PBS controls (Figure 3F). After the mice were euthanized, we examined the serum of each group for liver and renal functions, and we discovered that there were no significant differences in serum ALT (Figure 3B), AST (Figure 3C), BUN (Figure 3D), and Cr (Figure 3E) between the mice treated with different dosage groups and Control group. Furthermore, mice treated with several dose groups of HNVs and Control group did not significantly differ in their major organs, such as the heart, liver, spleen, lung, or kidney, according to HE staining (Figure 3A). These results suggest that HNVs are safe for biomedical applications.

HNVs Protect Against Pathological Symptoms Associated with ALF Mice

By injecting LPS/GalN intraperitoneally into BALB/c mice and then administering HNVs orally, we established an ALF model and confirmed the therapeutic effect of HNVs on ALF mice (Figure 4A). Treatment with HNVs significantly repaired the abnormal liver morphology observed in mice treated with LPS/GalN (Figure 4B). We then verified the safety of HNVs at the cellular level, and we discovered that HepG2 cells could maintain good cellular activity after treatment with different concentrations of HNVs (Figure 4C). Then, we evaluated the liver pathology in each group of mice by HE staining (Figure 4D), and we found that LPS/GalN induced disorganization of the liver, hepatocellular necrosis, and large-scale inflammatory cell infiltration, which was significantly improved by HNVs treatment. Since serum ALT and AST are considered to be crucial indicators for evaluating ALF, we measured the levels of these chemicals in mice.[24] We discovered that LPS/GalN increased serum levels of ALT (Figure 4E) and AST (Figure 4F) in mice. However, HNVs significantly decreased ALT and AST levels. In summary, HNVs were able to protect against pathological symptoms associated with ALF in mice, including improvement of liver morphology, histological disorganization, inflammatory cells infiltration, hepatocyte necrosis, and modulation of serum ALT and AST.

RNA-Seq Analysis of the Liver

Liver samples were used for RNA-Seq analysis. Comparative analysis of volcano plots of hepatic transcriptional profiles in the LPS/GalN+HNVs and LPS/GalN groups showed that significant up-regulation of 599 genes and significant down-regulation of 641 genes by HNVs (Figure 5A). This is further validated by a heat map of clustering between LPS/GalN +HNVs and LPS/GalN groups (Figure 5B). According to KEGG enrichment analysis (Figure 5C), we found that HNVs ameliorated ALF by participating in the regulation of several inflammatory immune pathways, including the Chemokine signaling pathway, MAPK signaling pathway, and TNF-α signaling pathway. Furthermore, GO enrichment analysis showed that HNVs up-regulated a variety of biological processes including cellular modified amino acid catabolic process, etc. (Figure 5D). At the same time HNVs downregulate biological processes such as chemokine-mediated signaling pathway, response to interleukin-1 and molecular functions such as CCR chemokine receptor binding, MAP kinase phosphatase activity, chemokine receptor activity, C-C chemokine binding (Figure 5E).

HNVs Inhibit M1 Polarization and Chemokine Recruitment

Based on KEGG (Figure 5C) and GO (Figure 5E) enrichment analyses in RNA-Seq, we found that HNVs improved ALF mainly by inhibiting inflammatory immune pathways. Thus, we applied flow cytometry to investigate the expression of pro-inflammatory M1 cells (CD45+CD11b+F4/80+CD11c+) and anti-inflammatory M2 cells (CD45+CD11b+F4/80 +CD206+) in the LPS/GalN+HNVs and LPS/GalN groups, respectively (Figure 6A). Quantitative analysis showed that LPS/GalN significantly up-regulated the expression of pro-inflammatory M1 cells compared to the Control group, which was significantly down-regulated by HNVs (Figure 6D). Furthermore, the significant reduction of anti-inflammatory M2 cells caused by LPS/GalN was significantly reversed by HNVs (Figure 6E). Then, using immunofluorescence staining, we confirmed that HNVs can prevent macrophage polarization toward M1 (Figure 6B) and encourage polarization toward M2 (Figure 6C). Quantitative analysis of immunofluorescence staining showed that HNVs significantly inhibited the significant expression of pro-inflammatory M1 cells in the liver caused by LPS/GalN (Figure 6F) and significantly up-regulated anti-inflammatory M2 cells in ALF mice (Figure 6G). Since, the high expression of pro-inflammatory M1 macrophages leads to the release of large amounts of chemokines from hepatic Kupffer cells in order to

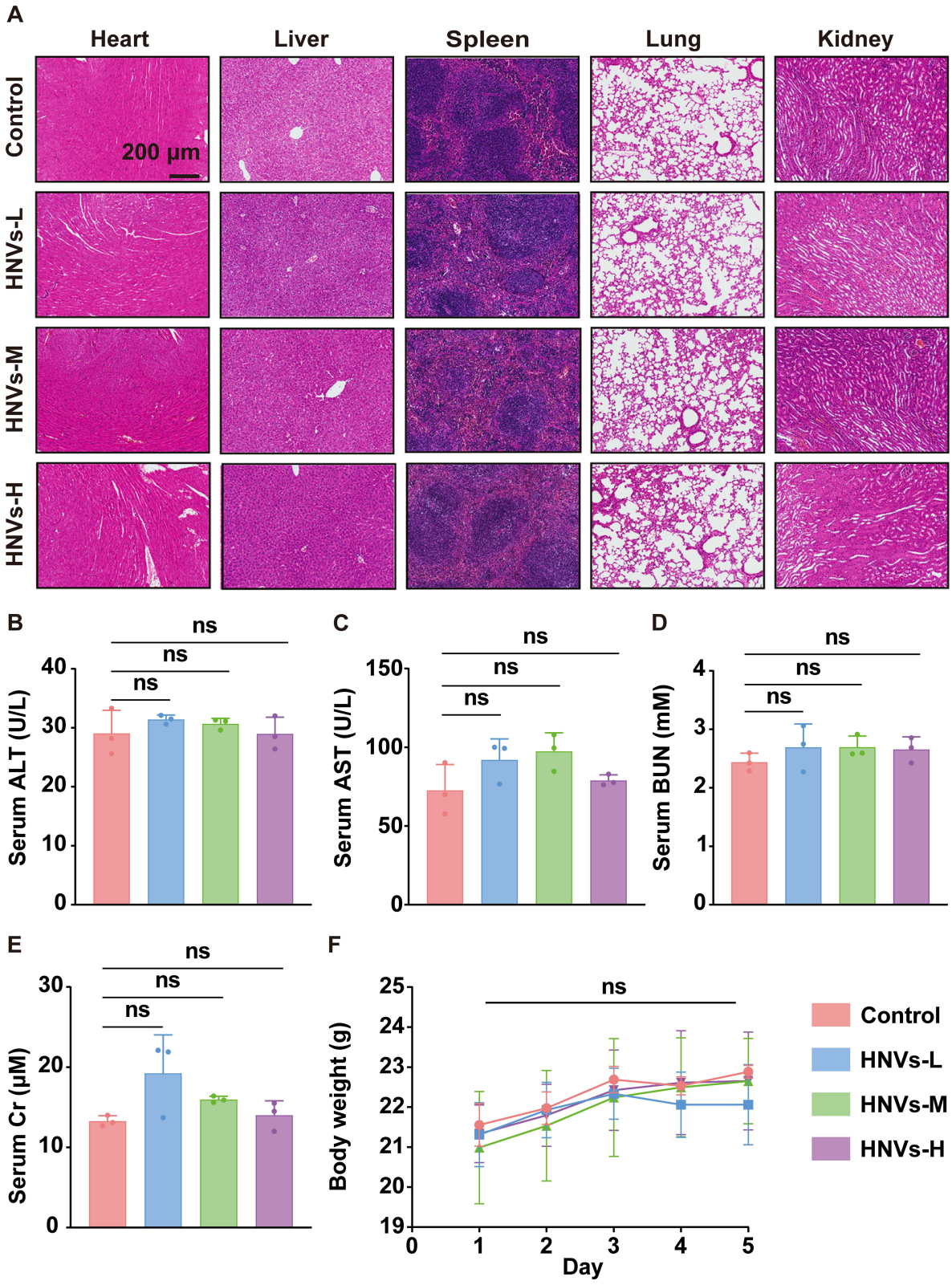

Figure 3 Biosafety Evaluation of HNVs. (**A**) HE images of the main organs of mice given varying HNVs doses. Serum ALT (**B**), AST (**C**), BUN (**D**), and Cr (**E**) levels in mice treated with various doses of HNVs. (**F**) Changes in body weight of mice treated with various doses of HNVs. Statistical analysis was performed using one-way ANOVA. Data were expressed as the mean ± SD (n=3 in each group). n.s., not significant vs Model group.
Abbreviations: HNVs-L, HNVs low-dose; HNVs-M, HNVs medium-dose; HNVs-H, HNVs high-dose.

https://doi.org/10.2147/IJN.S526819

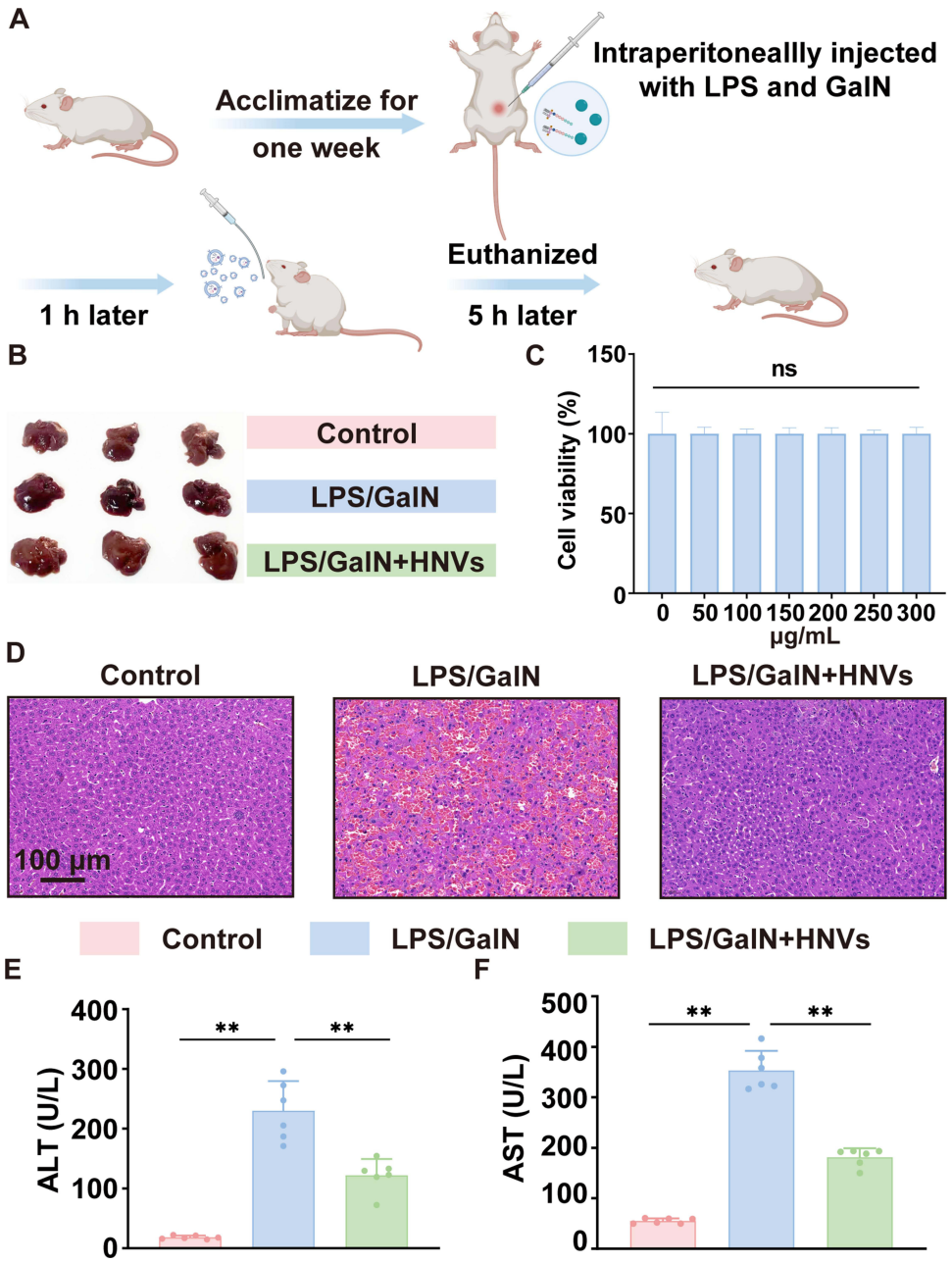

Figure 4 Therapeutic effect of HNVs on ALF. (**A**) Creation of an ALF mouse model and the HNVs therapy procedure. (**B**) Liver morphology of mice in each group (n=3 in each group). (**C**) Cell viability of HepG2 cells after treatment with different concentrations of HNVs (n=5 in each group). (**D**) HE Staining of Liver. (**E**) Serum ALT level in mice (n=6 in each group). (**F**) Serum AST level in mice (n=6 in each group). Statistical analysis was performed using one-way ANOVA. Data were expressed as the mean ± SD. * $P < 0.05$, ** $P < 0.01$, n.s., not significant vs Model group.

recruit chemokine receptors in the circulating blood, which results in the development of an inflammatory response.[25] Therefore, Quantitative real-time PCR was carried out to quantify chemokines and their receptors in liver tissues. The findings revealed that LPS/GalN considerably increased the levels of CCL2 (Figure 6H), CCR2 (Figure 6I), CCL5 (Figure 6J), and CCR5 (Figure 6K) in liver tissues compared to the Control group, which was markedly suppressed by HNVs, inhibiting the immune-inflammatory response.

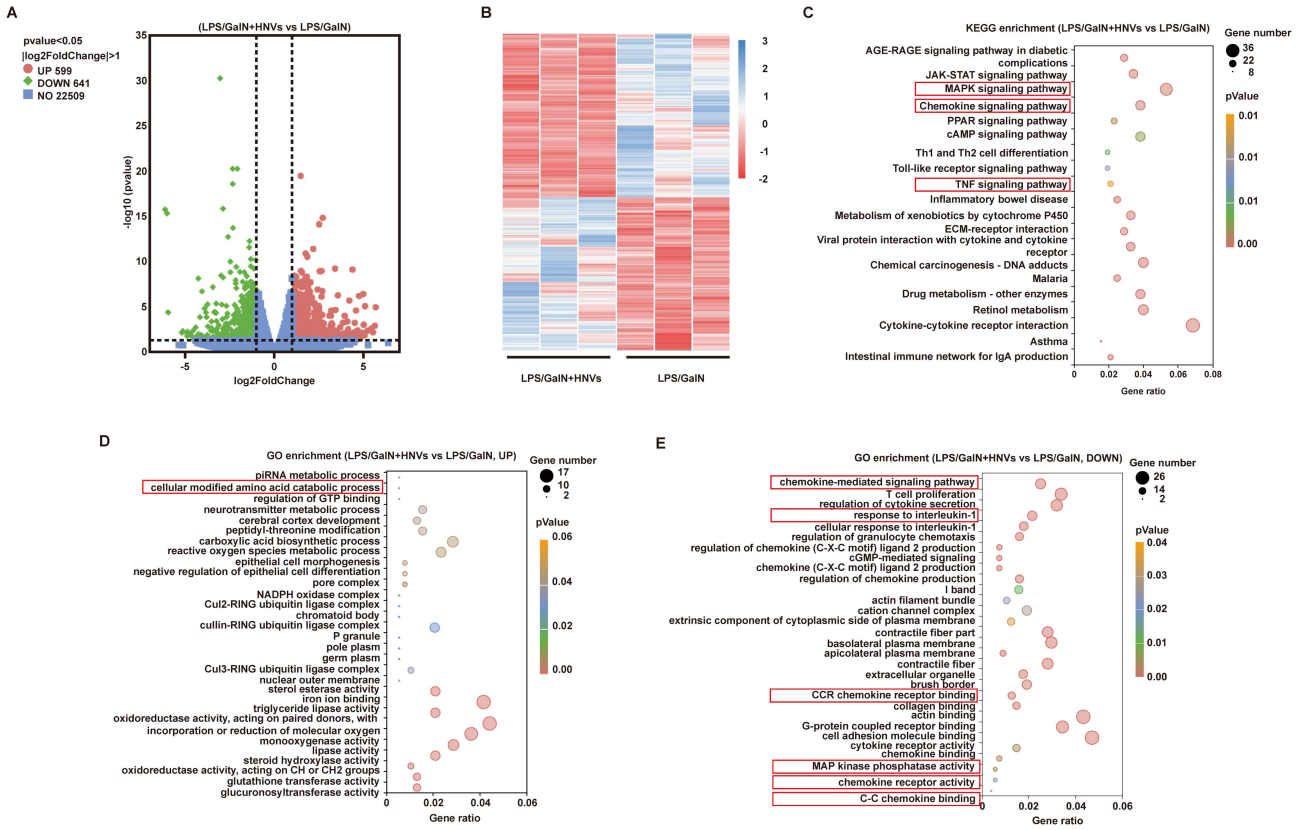

Figure 5 RNA-Seq analysis of the liver. (**A**) The volcano plot represents the gene expression differences between the LPS/GalN+HNVs group and the LPS/GalN group. The red dots and green dots represent the up- and down-regulation of differentially expressed genes in the LPS/GalN+HNVs group compared to the LPS/GalN group, respectively. The y-axis displays the significance of variations in gene expression, while the x-axis displays log2FoldChange. (**B**) Cluster analysis of the differences in expression profiles between LPS/GalN+HNVs and LPS/GalN. (**C**) 20 significantly enriched KEGG pathways. Gene ratio is shown on the X-axis, while the KEGG pathway is shown on the Y-axis. LPS/GalN+HNVs compared to LPS/GalN significantly up- (**D**) or down- (**E**) 20 GO terms. X-axis represents Gene ratio, Y-axis represents GO terms. (**C–E**) The size of the dots represents the number of genes associated with the KEGG pathway or GO terms.

HNVs Promote Autophagy and Inhibit Apoptosis Thereby Reducing Inflammatory Response

Autophagy is a cellular process that maintains intracellular homeostasis in cellular inflammation and injury.[26] Growing evidence that enhanced autophagy attenuates the immune-inflammatory response in ALF mice.[27,28] To determine the expression of genes linked to autophagy, we employed Western blotting. The findings indicated that P62 protein expression was significantly up-regulated and accompanied by a significant decrease in Atg5, Atg7 protein expression in contrast to the Control group, whereas HNVs were able to significantly reverse the effect of LPS/GalN on autophagy-related protein expression (Figure 7A), implying that HNVs can protect against the effects of ALF by enhancing autophagy. Moreover, apoptosis, a sort of programmed cell death is considered a prominent pathological feature of ALF.[29] According to Western blotting results, LPS/GalN dramatically increased the expression of P53 protein in liver tissues (Figure 7A). This trend was successfully reversed by HNVs therapy. We then performed immunofluorescence staining of the liver tissue using terminal deoxynucleotidyl transferase dUTP nick end labeling (TUNEL) (Figure 7H), which was used as a marker of apoptosis. Quantitative results showed (Figure 7I) that LPS/GalN significantly induced an increase in TUNEL expression in liver tissue, which was significantly reduced by HNVs. Next, we examined the expression of inflammatory factors in the serum of each group of mice using ELISA. The results showed that HNVs significantly reduced the expression of IL-6 (Figure 7B), IL-1β (Figure 7C), and TNF-α (Figure 7D) in ALF mice. We further performed quantitative real-time PCR for inflammatory factors in the liver tissues of mice in each group. Consistent with the results in serum, the significant upregulation of IL-6 (Figure 7E), IL-1β (Figure 7F), and TNF-α

https://doi.org/10.2147/IJN.S526819

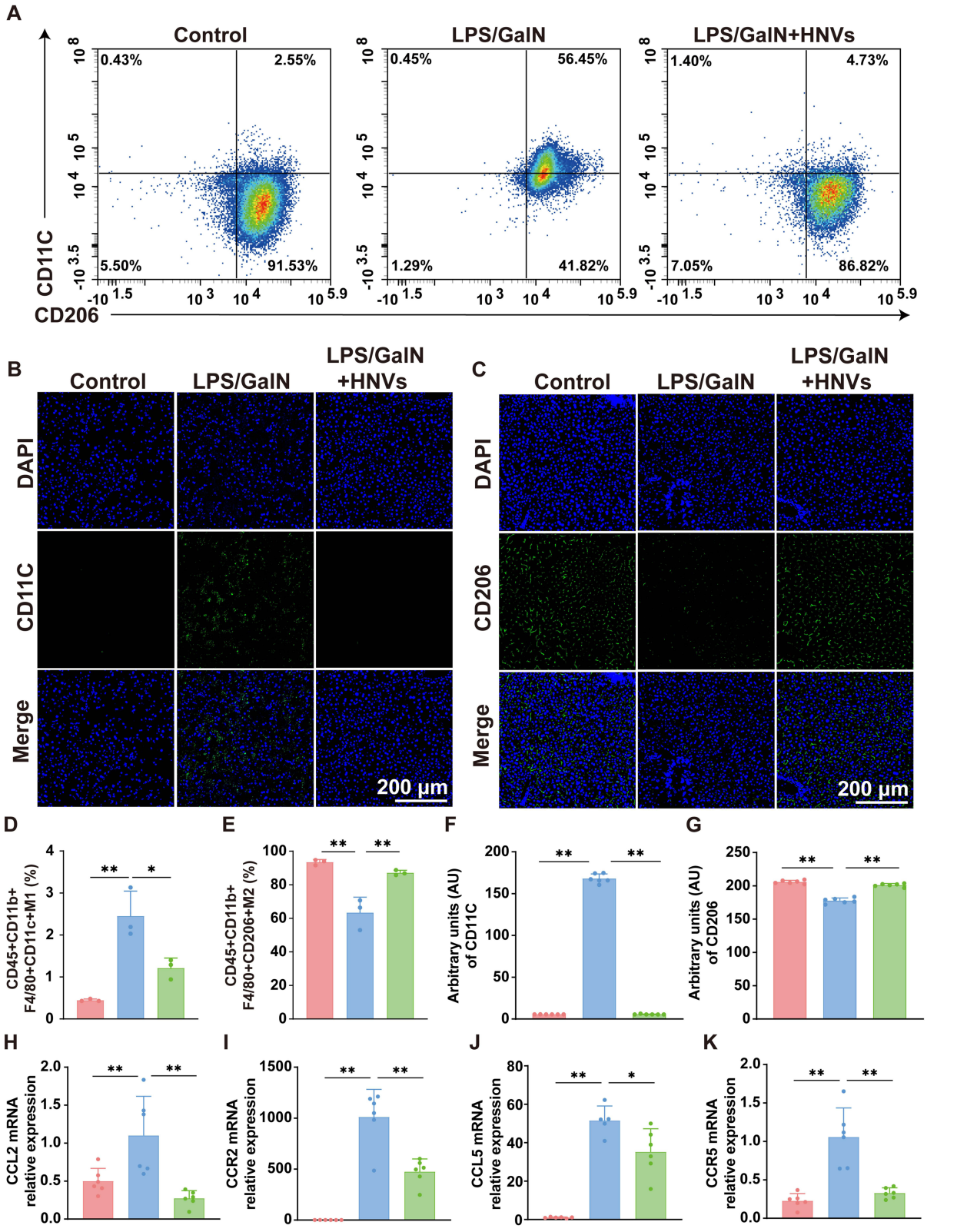

Figure 6 HNVs inhibit M1 polarization and chemokine recruitment. (**A**) Flow cytometry. (**B** and **C**) Representative images of CD11C and CD206 immunofluorescence staining in liver. (**D** and **E**) Quantification of M1 and M2 by flow cytometry (n=3 in each group). Quantification of CD11C (**F**) and CD206 (**G**) immunofluorescence staining in liver (n=6 in each group). Relative mRNA expression of chemokines CCL2 (**H**), CCR2 (**I**), CCL5 (**J**) and CCR5 (**K**) in liver tissues (n=6 in each group). Statistical analysis was performed by one-way ANOVA. Data were expressed as the mean ± SD. * $P < 0.05$, ** $P < 0.01$, n.s., not significant vs Model group.

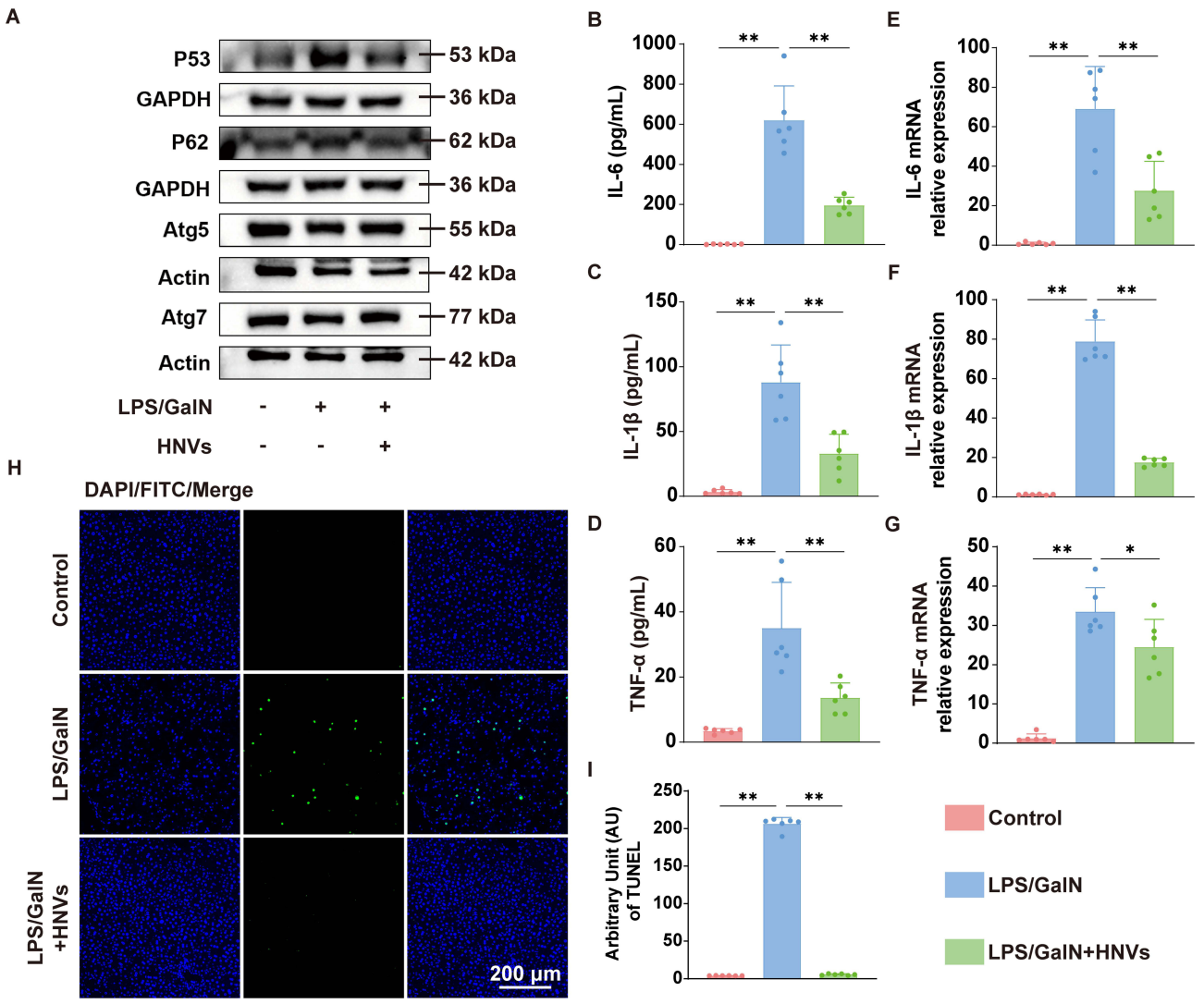

Figure 7 HNVs promote autophagy and inhibit apoptosis thereby reducing inflammatory response. (**A**) Western blotting results of p53, p62, Atg5, Atg7. (**B–D**) Expression of inflammatory factors IL-6, IL-1β and TNF-α in serum by ELISA (n=6 in each group). (**E–G**) Using quantitative real-time PCR to identify the liver's expression of the inflammatory factors IL-6, IL-1β and TNF-α (n=6 in each group). (**H**) TUNEL staining fluorogram. (**I**) Quantitative results of TUNEL staining (n=6 in each group). Statistical analysis was performed by one-way ANOVA. Data were expressed as the mean ± SD. * $P < 0.05$, ** $P < 0.01$, n.s., not significant vs Model group.

(Figure 7G) levels induced by LPS/GalN were effectively reversed by HNVs. The above results suggest that HNVs can enhance autophagy and inhibit apoptosis, which in turn suppresses the immune response.

HNVs Regulate LPS/GalN-Induced Alterations in the Gut Microbiota

According to studies, ALF is typically accompanied by a gut microbiota imbalance,[30] which further damages the intestinal barrier, allowing enteric LPS to enter the liver through the portal vein, resulting in a cascade of immune-inflammatory responses that further exacerbate ALF.[31] Therefore, to examine the variations in the gut microbiota composition among each group, we used 16s rRNA. Based on the Upset and Venn diagrams, we found that the three groups shared 425 identical amplicon sequence variations (ASVs), while 938 ASVs were present only in LPS/GalN+HNVs (Figure 8A). To evaluate the variations in the α-diversity of the gut microbiota across the groups, the Ace, Chao, Shannon, and Simpson indices were employed (Figure 8B); however, these four indices were not significantly different among the three groups. We then analyzed the β-diversity of the gut microbiota in each group of mice using principal coordinate analysis (PCOA) based on Bray Curtis and weighted unifrac (Figure 8C), the results showed that HNVs treatment brought the composition of the gut microbiota significantly closer to that of Control group and significantly separated it from that of the gut microbiota in LPS/

https://doi.org/10.2147/IJN.S526819

GalN group. Next, we analyzed the relative abundance of the gut microbiota in three groups of mice. Figure 8D shows the top 10 microbial levels at the phylum level for each group of mice. We detected that LPS/GalN decreased the relative abundance of *Firmicutes* and upregulated the relative abundance of *Desulfobacterota*, while HNVs treatment was able to significantly reverse this trend (Figure 8E). Figure 8F shows the top 20 microbial levels at the genus level for each group of mice. In LPS/GalN-induced mice, we noticed that the relative abundance of *Bacillus* and *Lactobacillus* had decreased, whereas treatment with HNVs dramatically increased the levels of *Lactobacillus* and *Bacillus* (Figure 8G). Next, we investigated the differences between the gut microbiota of the LPS/GalN group and the LPS/GalN+HNVs group using LDA effect size (LEfse) (Figure 8H). Enriched in LPS/GalN were mainly *Desulfobacterota* at the phylum level and *Desulfovibrio* at the genus level, whereas enriched in LPS/GalN+HNVs were mainly *Firmicutes* at the phylum level and *Lactobacillus, Bacillus Lachnospiraceae_FCS020_group* at the genus level.

Discussion

Compared to exosome-like nanovesicles of mammalian origin, the extraction process of exosome-like nanovesicles (PELNVs) of plant origin is simple, inexpensive and suitable for large-scale production.[32] In addition, due to their natural origin, PELNVs are low immunogenic, non-toxic and highly biocompatible.[18,33,34] Moreover, PELNVs exhibit superior targeting capability and higher bioavailability relative to traditional botanical drugs, which may result in comparable or

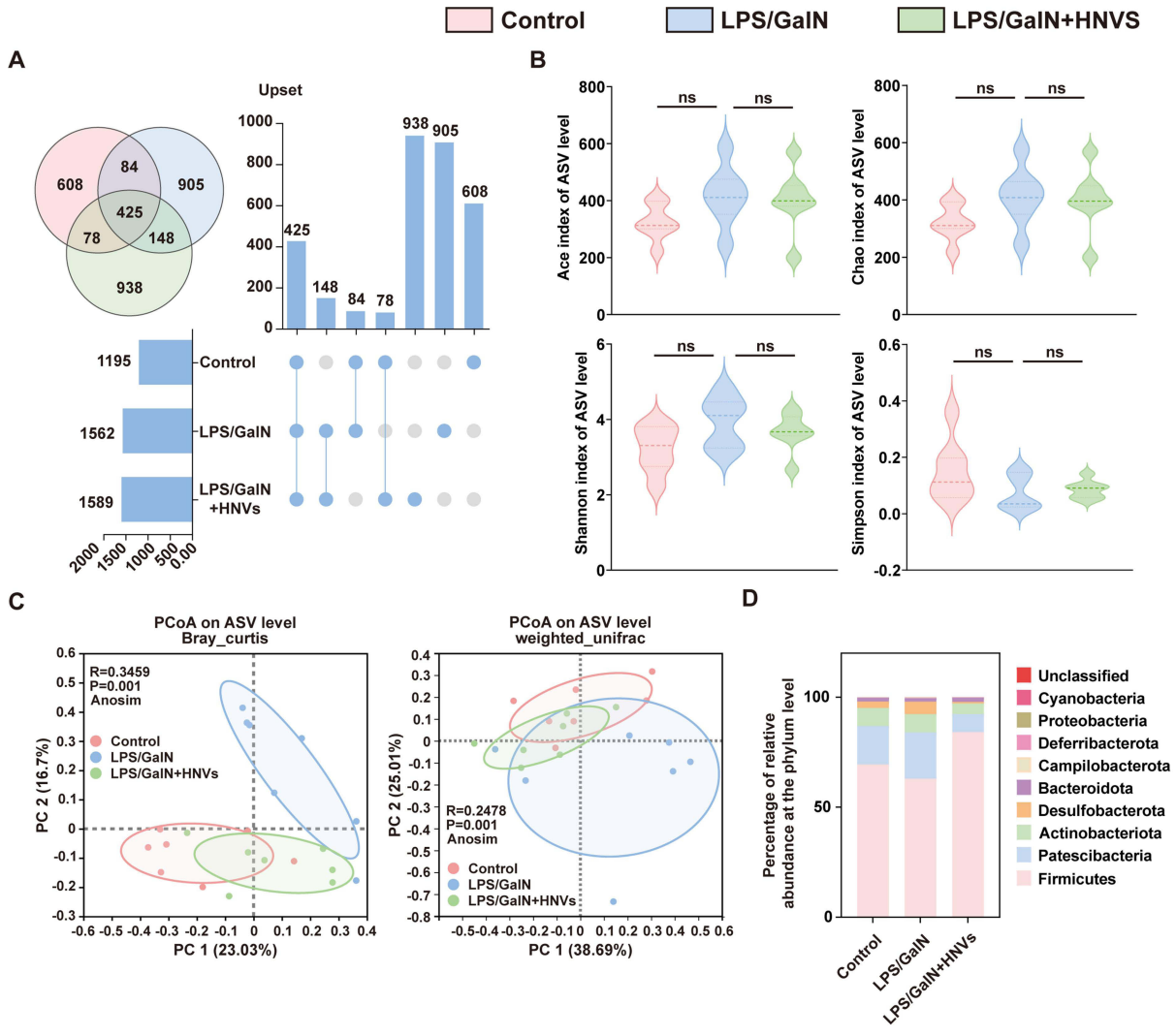

Figure 8 Continued.

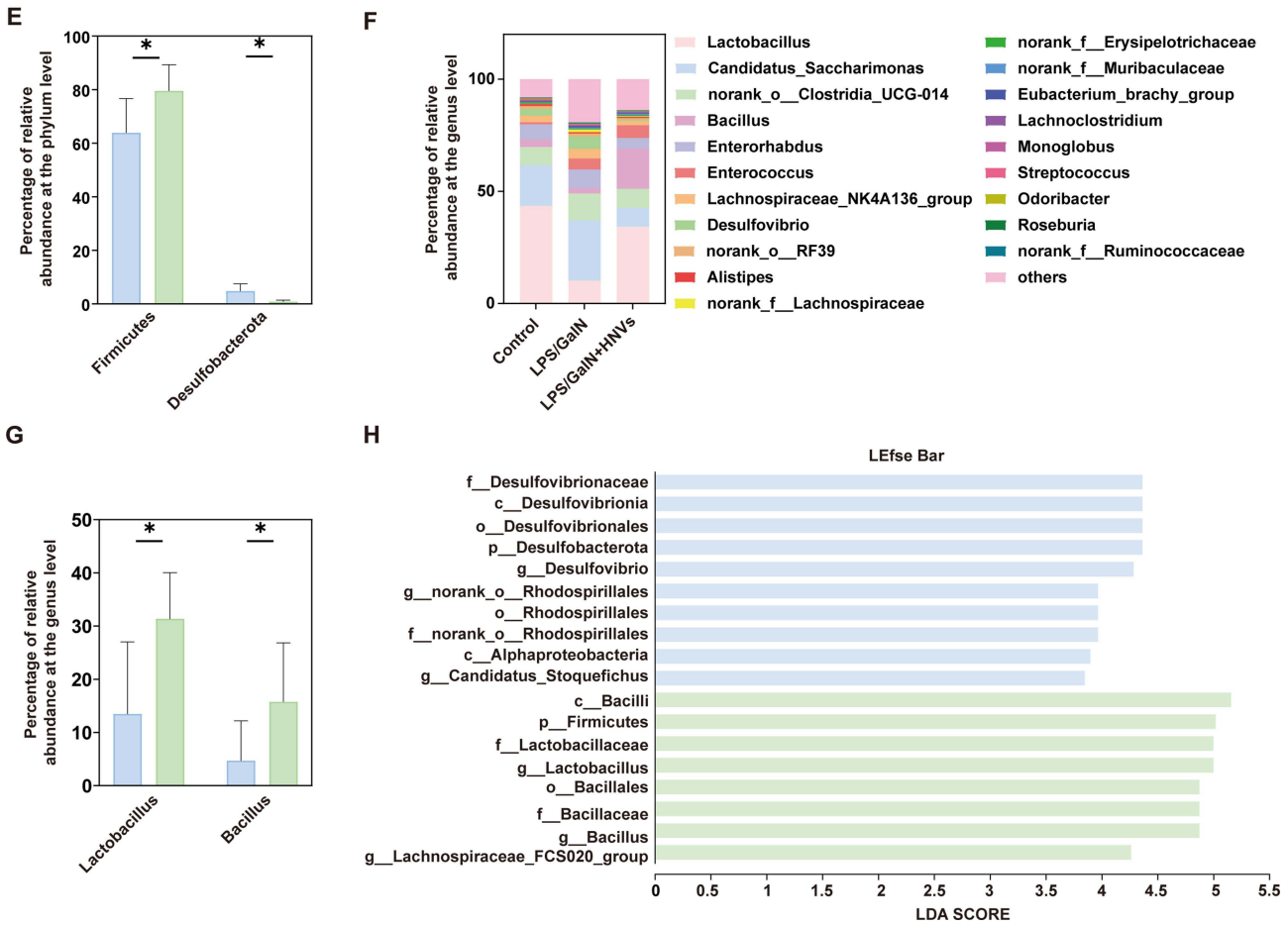

Figure 8 16s rRNA analysis. n = 7 individuals/group. (**A**) Upset and Venn diagram. (**B**) The α-diversity of Ace, Chao, Shannon and Simpson indices. (**C**) PCoA analysis based on Bray curtis and weighted unifrac, differences of data were calculated by Anosim test. (**D**) Percentage of relative abundance at the phylum level. (**E**) Percentage of relative abundance of *Firmicutes* and *Desulfobacterota*. (**F**) Percentage of relative abundance at the genus level. (**G**) Percentage of relative abundance of *Lactobacillus* and *Bacillus*. (**H**) LEfse analysis of predominant biomarkers in the LPS/GalN and LPS/GalN+HNVs groups. The threshold of the score of LDA analysis was 4.0. Data were expressed as the mean ± SD. * $P < 0.05$, ** $P < 0.01$, n.s., not significant vs Model group.

enhanced therapeutic efficacy.[35,36] Previously, PELNVs have already been shown to be effective in a variety of animal models, such as garlic exosomes for the alleviation of acute liver injury,[24] rhubarb exosomes for the alleviation of acute lung injury,[37] and ginseng exosomes for the amelioration of colitis.[38]

Here, we extracted plant-derived exosome-like nanovesicles from the traditional Chinese herb Honeysuckle and explored its efficacy and mechanism in ALF. We first validated the characterisation of HNVs, which we found to be individual exosome-like nanovesicles with a spherical morphology in the range of 50–200 nm, with a particle size distribution around 158.5 nm and a potential of −15.97 mV, as measured by Cryo-EM and DLS. Then by simulating the environment of the human digestive tract, we found that HNVs were able to maintain excellent stability in the gastrointestinal tract, which lays a good foundation for the subsequent ability of HNVs to be used in the treatment of ALF by oral gavage. Before exploring the efficacy and mechanism of HNVs in the treatment of ALF, we performed a biosafety evaluation of HNVs. After 5 days of treatment with HNVs in different dosage groups, there were no significant differences in histopathological conditions, liver functions, kidney functions, and body weights between groups of mice, indicating that HNVs are safe and effective as natural nanomedicines. Next, our study demonstrated that HNVs effectively protected against liver tissue structure damage, hepatocyte necrosis and massive inflammatory cell infiltration in ALF mice while significantly reducing LPS/GalN-induced massive expression of serum ALT, AST, suggesting a favourable ameliorative effect of HNVs on ALF.

https://doi.org/10.2147/IJN.S526819

Following that, we employed RNA-Seq to investigate how HNVs improve ALF. According to KEGG and GO enrichment, HNVs improve ALF by blocking chemokine recruitment and decreasing inflammatory responses. In ALF model, hepatic Kupffer cells often exhibit pro-inflammatory M1 polarization, which exacerbates the process of liver injury by releasing chemokines to recruit chemokine receptors in blood monocytes, creating an immune-inflammatory response.[39] Thus, flow cytometry and immunofluorescence staining were used to confirm that HNVs greatly prevented the polarization of hepatic Kupffer cells to M1 macrophages. Next, we verified that HNVs inhibit the recruitment of the chemokines CCL2, CCR2, CCL5, and CCR5 utilizing Quantitative Real-time PCR. Given the critical roles that autophagy and apoptosis play in the inflammatory immune response, we confirmed using Western blotting and immunofluorescence staining that HNVs can improve ALF by promoting autophagy, preventing apoptosis, and thereby lowering the blood and liver's expression of inflammatory factors.

In the in vivo distribution experiments of HNVs, we can observe that HNVs were unable to reach the liver in Control group, whereas in ALF mice, HNVs were able to pass through the intestines and enter the liver. We hypothesize that this could be related to impairment to the intestinal barrier in ALF mice. Gut microbiota abnormalities have been demonstrated to cause intestinal barrier impairment, which allows the microbial metabolite LPS to enter the liver through the compromised barrier and exacerbate ALF.[40,41] Therefore, we performed 16s rRNA analyses. The findings demonstrated that the gut microbiota composition of ALF mice was significantly different from that of the Control group and that LPS/GalN decreased the genus-level abundance of Lactobacillus and Bacillus. These trends were significantly reversible by the administration of HNVs. Moreover, it has been shown that Lactobacillus and Bacillus may be associated with intestinal barrier repair.[42,43] It suggests that HNVs can regulate the disordered intestinal microbiota in ALF mice and thus repair the damaged intestinal barrier to inhibit the entry of intestinal metabolite LPS into the liver and thus suppress the immune-inflammatory response.

Thus, we hypothesized that HNVs exert their protective effects through dual pathways in the ALF mouse model: on the one hand, it reduces leakage of gut-derived LPS to the liver by regulating the intestinal microbiota and repairing the intestinal barrier function; on the other hand, HNVs can enter the liver via the damaged intestinal barrier and directly inhibit exogenous LPS-induced liver injury.

In conclusion, we developed a naturally-derived nanomedicine, HNVs, and validated its remarkable therapeutic effect in an LPS/GalN-induced ALF mouse model. Based on their favorable biosafety, excellent oral stability, and well-defined therapeutic mechanisms, HNVs show good prospects for clinical translation. Future studies will focus on the development of its GMP-grade manufacturing process, the optimization of different delivery strategies (especially the clinical translational pathway for oral administration), and more in-depth long-term safety evaluations to accelerate its advancement to clinical applications. In addition, given the high mortality rate of ALF and the limitations of current effective treatments, the successful development and translation of HNVs, which are safe, effective and orally available therapies, is expected to provide new therapeutic options for patients with ALF and significantly improve their survival and quality of life, which is potentially important for the maintenance of human liver health.

Nevertheless, for our study, we have the following shortcomings: ALF is a clinical syndrome caused by multiple factors. However, only the LPS/GalN-induced ALF model was used in this study to assess the role of HNVs. Multiple ALF models are needed in the future to comprehensively assess the broad applicability of HNVs to ALF.

Data Sharing Statement

The data that support the findings of this study are available from the corresponding author upon reasonable request.

Supplementary Materials

List of Quantitative real-time PCR primer sets (mouse).

Disclosure

The authors declare that they have no competing interests.

References

1. Maiwall R, Kulkarni AV, Arab JP, Piano S. Acute liver failure. *Lancet*. 2024;404(10454):789–802. doi:10.1016/s0140-6736(24)00693-7
2. Stravitz RT, Lee WM. Acute liver failure. *Lancet*. 2019;394(10201):869–881. doi:10.1016/s0140-6736(19)31894-x
3. Kheradpezhouh E, Ma L, Morphett A, Barritt GJ, Rychkov GY. TRPM2 channels mediate Acetaminophen-induced liver damage. *Proc Natl Acad Sci USA*. 2014;111(8):3176–3181. doi:10.1073/pnas.1322657111
4. Galanos C, Freudenberg MA, Reutter W. Galactosamine-induced sensitization to the lethal effects of endotoxin. *Proc Natl Acad Sci USA*. 1979;76 (11):5939–5943. doi:10.1073/pnas.76.11.5939
5. Seki E, Brenner DA. Toll-like receptors and adaptor molecules in liver disease: update. *Hepatology*. 2008;48(1):322–335. doi:10.1002/hep.22306
6. Tripathi A, Debelius J, Brenner DA, et al. The gut-liver axis and the intersection with the microbiome. Review. *Nat Rev Gastroenterol Hepatol*. 2018;15(7):397–411. doi:10.1038/s41575-018-0011-z
7. Chopyk DM, Grakoui A. Contribution of the intestinal microbiome and gut barrier to hepatic disorders. *Gastroenterology*. 2020;159(3):849–863. doi:10.1053/j.gastro.2020.04.077
8. Yan M, Man S, Sun B, et al. Gut liver brain axis in diseases: the implications for therapeutic interventions. *Signal Transduct Target Ther*. 2023;8 (1):443. doi:10.1038/s41392-023-01673-4
9. Wu G, Win S, Than TA, Chen P, Kaplowitz N. Gut microbiota and liver injury (I)-acute liver injury. *Adv Exp Med Biol*. 2020;1238:23–37. doi:10.1007/978-981-15-2385-4_3
10. Liu B, Lu Y, Chen X, et al. Protective role of shiitake mushroom-derived exosome-like nanoparticles in D-galactosamine and lipopolysaccharide-induced acute liver injury in mice. *Nutrients*. 2020;12(2). doi:10.3390/nu12020477
11. Yan R, Wang K, Wang Q, et al. Probiotic Lactobacillus casei Shirota prevents acute liver injury by reshaping the gut microbiota to alleviate excessive inflammation and metabolic disorders. *Microb Biotechnol*. 2022;15(1):247–261. doi:10.1111/1751-7915.13750
12. Feng Q, Huang Z, Su L, Fan Y, Guan Y, Zhang G. Therapeutic efficacy and safety of Yinzhihuang granules with phototherapy in neonatal pathologic jaundice: an updated systematic review and meta-analysis. *Phytomedicine*. 2022;100:154051. doi:10.1016/j.phymed.2022.154051
13. Jeong SH, Park MY, Bhosale PB, et al. Potential antioxidant and anti-inflammatory effects of Lonicera japonica and Citri Reticulatae Pericarpium Polyphenolic Extract (LCPE). *Antioxidants*. 2023;12(8):1582. doi:10.3390/antiox12081582
14. Li W, Ding J, Chen S, et al. Alleviation of colitis by honeysuckle MIR2911 via direct regulation of gut microbiota. *J Control Release*. 2024;376:123–137. doi:10.1016/j.jconrel.2024.09.050
15. Zhao B, Lin H, Jiang X, et al. Exosome-like nanoparticles derived from fruits, vegetables, and herbs: innovative strategies of therapeutic and drug delivery. *Theranostics*. 2024;14(12):4598–4621. doi:10.7150/thno.97096
16. Bai C, Liu J, Zhang X, et al. Research status and challenges of plant-derived exosome-like nanoparticles. *Biomed Pharmacother*. 2024;174:116543. doi:10.1016/j.biopha.2024.116543
17. Jin Z, Na J, Lin X, Jiao R, Liu X, Huang Y. Plant-derived exosome-like nanovesicles: a novel nanotool for disease therapy. *Heliyon*. 2024;10(9): e30630. doi:10.1016/j.heliyon.2024.e30630
18. Mu N, Li J, Zeng L, et al. Plant-derived exosome-like nanovesicles: current progress and prospects. *Int J Nanomed*. 2023;18:4987–5009. doi:10.2147/ijn.S420748
19. Jin E, Yang Y, Cong S, et al. Lemon-derived nanoparticle-functionalized hydrogels regulate macrophage reprogramming to promote diabetic wound healing. *J Nanobiotechnol*. 2025;23(1):68. doi:10.1186/s12951-025-03138-y
20. Li JH, Xu J, Huang C, et al. Houttuynia cordata-derived exosome-like nanoparticles mitigate colitis in mice via inhibition of the NLRP3 signaling pathway and modulation of the gut microbiota. *Int J Nanomed*. 2024;19:13991–14018. doi:10.2147/ijn.S493434
21. Kim J, Zhu Y, Chen S, et al. Anti-glioma effect of ginseng-derived exosomes-like nanoparticles by active blood-brain-barrier penetration and tumor microenvironment modulation. *J Nanobiotechnol*. 2023;21(1):253. doi:10.1186/s12951-023-02006-x
22. Ou X, Wang H, Tie H, et al. Novel plant-derived exosome-like nanovesicles from Catharanthus roseus: preparation, characterization, and immunostimulatory effect via TNF-α/NF-κB/PU.1 axis. *J Nanobiotechnol*. 2023;21(1):160. doi:10.1186/s12951-023-01919-x
23. Zhang S, Wang Q, Tan DEL, et al. Gut-liver axis: potential mechanisms of action of food-derived extracellular vesicles. *J Extracell Vesicles*. 2024;13(6):e12466. doi:10.1002/jev2.12466
24. Zhao X, Yin F, Fu L, et al. Garlic-derived exosome-like nanovesicles as a hepatoprotective agent alleviating acute liver failure by inhibiting CCR2/ CCR5 signaling and inflammation. *Biomater Adv*. 2023;154:213592. doi:10.1016/j.bioadv.2023.213592
25. Cao S, Liu M, Sehrawat TS, Shah VH. Regulation and functional roles of chemokines in liver diseases. *Nat Rev Gastroenterol Hepatol*. 2021;18 (9):630–647. doi:10.1038/s41575-021-00444-2
26. Levine B, Kroemer G. Biological functions of autophagy genes: a disease perspective. *Cell*. 2019;176(1–2):11–42. doi:10.1016/j.cell.2018.09.048
27. Lin X, Cui M, Xu D, et al. Liver-specific deletion of Eva1a/Tmem166 aggravates acute liver injury by impairing autophagy. *Cell Death Dis*. 2018;9 (7):768. doi:10.1038/s41419-018-0800-x
28. Lin D, Chen H, Xiong J, et al. Mesenchymal stem cells exosomal let-7a-5p improve autophagic flux and alleviate liver injury in acute-on-chronic liver failure by promoting nuclear expression of TFEB. *Cell Death Dis*. 2022;13(10):865. doi:10.1038/s41419-022-05303-9
29. Wang H, Xu DX, Lu JW, Zhao L, Zhang C, Wei W. N-acetylcysteine attenuates lipopolysaccharide-induced apoptotic liver damage in D-galactosamine-sensitized mice. *Acta Pharmacol Sin*. 2007;28(11):1803–1809. doi:10.1111/j.1745-7254.2007.00657.x
30. Fuchs CD, Simbrunner B, Baumgartner M, Campbell C, Reiberger T, Trauner M. Bile acid metabolism and signalling in liver disease. *J Hepatol*. 2025;82(1):134–153. doi:10.1016/j.jhep.2024.09.032
31. Donnelly MC, Hayes PC, Simpson KJ. Role of inflammation and infection in the pathogenesis of human acute liver failure: clinical implications for monitoring and therapy. *World J Gastroenterol*. 2016;22(26):5958–5970. doi:10.3748/wjg.v22.i26.5958
32. Kim J, Li S, Zhang S, Wang J. Plant-derived exosome-like nanoparticles and their therapeutic activities. *Asian J Pharm Sci*. 2022;17(1):53–69. doi:10.1016/j.ajps.2021.05.006
33. Liu Y, Ren C, Zhan R, et al. Exploring the potential of plant-derived exosome-like nanovesicle as functional food components for human health: a review. *Foods*. 2024;13(5). doi:10.3390/foods13050712
34. Dad HA, Gu TW, Zhu AQ, Huang LQ, Peng LH. Plant exosome-like nanovesicles: emerging therapeutics and drug delivery nanoplatforms. review. *Mol Ther*. 2021;29(1):13–31. doi:10.1016/j.ymthe.2020.11.030

35. Yang Y, Yang L, Deng H, et al. Coptis chinensis-derived extracellular vesicle-like nanoparticles delivered miRNA-5106 suppresses NETs by restoring zinc homeostasis to alleviate colitis. *J Nanobiotechnol*. 2025;23(1):444. doi:10.1186/s12951-025-03466-z
36. Bethi CMS, Kumar MN, Kalarikkal SP, Narayanan J, Sundaram GM. Fenugreek-derived exosome-like nanovesicles containing bioavailable phytoferritin for the management of iron deficiency anemia. *Food Chem*. 2025;490:145088. doi:10.1016/j.foodchem.2025.145088
37. Qiu FS, Wang JF, Guo MY, et al. Rgl-exomiR-7972, a novel plant exosomal microRNA derived from fresh Rehmanniae Radix, ameliorated lipopolysaccharide-induced acute lung injury and gut dysbiosis. *Biomed Pharmacother*. 2023;165:115007. doi:10.1016/j.biopha.2023.115007
38. Kim J, Zhang S, Zhu Y, Wang R, Wang J. Amelioration of colitis progression by ginseng-derived exosome-like nanoparticles through suppression of inflammatory cytokines. *J Ginseng Res*. 2023;47(5):627–637. doi:10.1016/j.jgr.2023.01.004
39. Zhou Z, Pan X, Li L. Crosstalk between liver macrophages and gut microbiota: an important component of inflammation-associated liver diseases. *Front Cell Develop Biol*. 2022;10:1070208. doi:10.3389/fcell.2022.1070208
40. Krenkel O, Tacke F. Liver macrophages in tissue homeostasis and disease. *Nat Rev Immunol*. 2017;17(5):306–321. doi:10.1038/nri.2017.11
41. Jones RM, Neish AS. Gut microbiota in intestinal and liver disease. *Ann Rev Pathol*. 2021;16:251–275. doi:10.1146/annurev-pathol-030320-095722
42. Dempsey E, Corr SC. Lactobacillus spp. for gastrointestinal health: current and future perspectives. *Front Immunol*. 2022;13:840245. doi:10.3389/fimmu.2022.840245
43. Sun X, Yun L, Xie K, et al. Probiotic bacillus pumilus LV149 enhances gut repair, modulates microbiota, and alters transcriptome in DSS-induced colitis mice. *Front Microbiol*. 2024;15:1507979. doi:10.3389/fmicb.2024.1507979